Plasmonics (2018) 13:1811–1816
https://doi.org/10.1007/s11468-018-0695-5

Nanoantenna-Enhanced Radiative and Anisotropic Decay Rates in Monolayer-Quantum Dots

Laxmi Narayan Tripathi[1,2] · **M. Praveena**[2] · **Ben Johns**[2] · **Jaydeep Kumar Basu**[2]

Received: 20 August 2017 / Accepted: 3 January 2018 / Published online: 12 January 2018

Abstract
Nanoantenna-enhanced ultrafast emission from colloidal quantum dots as quantum emitters is required for fast quantum communications. On-chip integration of such devices requires a scalable and high-throughput technology. We report self-assembly lithography technique of preparing hybrid of gold nanorods antenna over a compact CdSe quantum dot monolayer. We demonstrate resonant and nonresonant gold nanorod antenna-enhanced radiative and anisotropic decay. Extensive simulations explain the mechanism of the decay rates and the role of antenna in both random and compact monolayers of quantum dots. The study could find applications in quantum dot display and quantum communication devices.

Keywords Nanoantena · Quantum dots · Plasmonics

Introduction

Colloidal quantum dots (QDs) are known to be single-photon emitters [1] and are desperately needed for quantum communications, quantum information processing, quantum computers, etc. Optical antenna [2, 3] has been shown to enhance the spontaneous emission [4] as well as ultrafast emission [1] through radiative decay rate enhancement of the photons for fast quantum communication. Resonant excitation of optical antennas such as metal nanoparticles/rods enhances the electromagnetic field dramatically via localized surface plasmon resonance [3, 5, 6]. A single QD can experience this strong electromagnetic environment via coupling to this surface plasmon modes, provided QDs lie within the penetration depth of electric field of surface plasmon [7]. The decay rate of the QDs can be significantly modified by the resonant excitation of QDs and metal nanoantenna [8, 9]. Fabrication of aligned and isolated optical antenna over monolayer QDs is an important step in realization of such optical interaction. We need a high-throughput and scalable technology to fabricate preferably aligned optical antenna over a compact monolayer of QDs.

Here, we provide optimum physical parameters to transfer such antenna over monolayer of QDs. We combine a directed self-assembly technology using Langmuir-Blodgett (LB) [10–12] and controlled dip coating, a high-throughput and scalable method. A controlled dip coating provides a better scheme in transferring aligned GNRs. In the dip coating process, a known concentration, C (mg/ml) of CTAB capped GNRs in water and a KSV mini trough (Finland) dipper were used to insert a QD film inside the GNR solutions, waited for dip time, τ, and then taken out with speed, u. We have optimized the condition for transfer of aligned GNRs from water. The parameters like dipping time (τ), dipping speed (u), and area fraction (ϕ) are given in the Table 1. The dipping method imparts an overall directionality to the GNR, along the dipping direction while the density of GNRs was controlled by the dipping speed and density of GNR solutions. Recently, we have also shown long-range emission enhancement [12] due to resonant optical antenna from a monolayer of QDs. Here, we demonstrate radiative decay rate enhancements from a monolayer of QDs due to isolated and aligned optical antenna. We have performed extensive finite difference time domain (FDTD) calculations for decay rate enhancements of a dipole emitter as a function of separation from both resonant and non resonant antenna.

✉ Laxmi Narayan Tripathi
nara.laxmi@gmail.com

[1] Julius Maximilians Universitat, Wuerzburg, Germany

[2] Department of Physics, Indian Institute of Science, Bangalore, India

Table 1 Optimum parameters for transfer of aligned GNRs on a CdSe QD monolayer

Sample[1] index	C[1] (mg/ml)	τ[2] (min)	u[3] (mm/min)	ϕ[4] (%)
S_1	0.003	1	10	1.04
S_2	0.003	15	10	2.64
S_3	0.003	30	10	3.94
S_4	0.006	1	10	1.63
S_5	0.006	15	10	2.51
S_6	0.006	30	10	6.25
S_7	0.012	1	10	5.89
S_8	0.012	15	10	7.10
S_9	0.012	30	10	9.21

[1]Concentration of CTAB capped GNRs in milligrams per milliliter in water

[2]Time duration which the substrate was inside water

[3]Speed of the dipper with respect to water

[4]Fraction of area covered by GNRs on the QD monolayer was calculated from TEM images using Image J software

Experimental Methods

To prepare a monolayer of CdSe quantum dots (QDs), we synthesized CdSe QDs of mean core diameter of 10 nm (Fig. 1b) with emission wavelength of 650 nm, using method developed by Peng et al. [13]. Photoluminescence (PL) spectrum for the QDs is shown in Fig. 1a. Gold nanorods (GNRs) of aspect ratios (AR) 2 and 3, hereafter, referred as AR2 and AR3 respectively, were chemically synthesized using methods as described earlier [12, 14]. The shape and size of GNR were estimated using transmission electron microscope (TEM) micrograph. The concentrations of GNR in water were determined from inductively coupled plasma optical emission spectroscopy (ICP-OES) (Perkin-Elmer). The UV-visible absorption data were used to estimate the concentration of GNRs in a diluted solution. The absorption spectra of thin film of GNRs with AR2 and AR3 are shown in Fig. 1a. We can see that the longitudinal surface plasmon resonance (LSPR) peak of AR 2 is overlapping with emission peak of CdSe QDs; therefore, we call AR2 GNRs as resonant antenna. Similarly, LSPR peak of AR3 GNR is not overlapping with PL of QDs; hence, we call it off-resonant GNR antenna.

We transferred a compact LB monolayer of CdSe QDs and used it as substrate to transfer an aligned layer of GNR by dipping it for 1 min inside a GNR solution. Then, it was pulled out in a controlled way using a dipper at the rate of 10 mm/min. To transfer low number density of GNR over the film, concentration of GNRs in the solution was intentionally kept low ($\equiv$ 0.01 mg/ml). The film was then dried in vacuum for 12 h. Transfer and orientation of rods along the dipping direction was confirmed by AFM. The typical ratio of GNR to QD was found to be 1:800. Table 1 shows different set of physical parameters for aligned and isolated GNR antenna transfer. Let us define hybrid of GNR with AR2 as A1 and hybrid of GNR with AR3 as A2. We

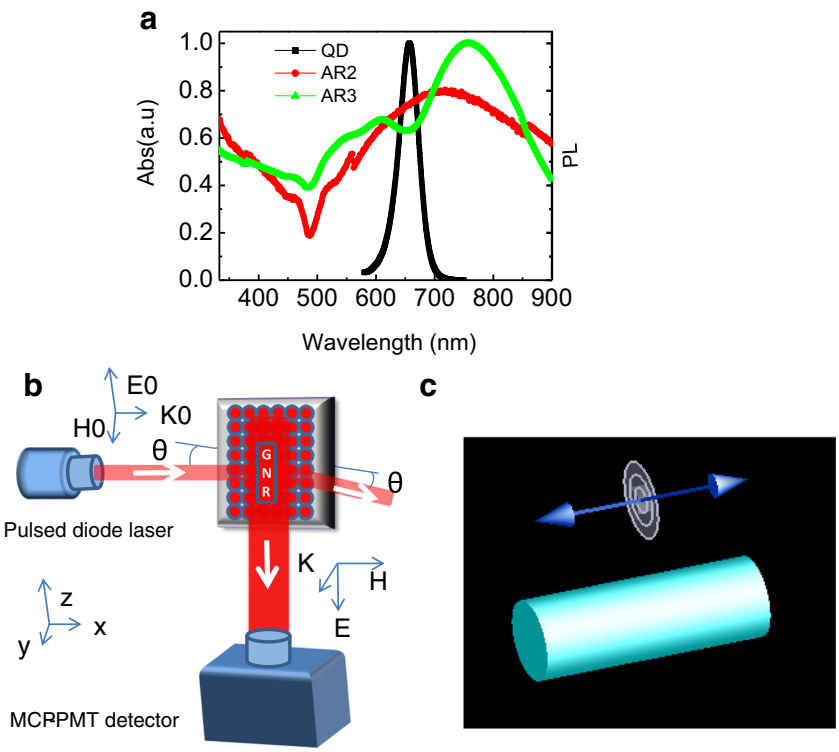

Fig. 1 **a** Absorption spectra of dense film of GNR antenna, both AR2; AR3 and PL spectrum of CdSe QDs in toluene. **b** TCSPC set up: a pulsed 633-nm diode laser and showing the **p** polarization of excitation and emission and a micro-channel plate-photomultiplier (MCP-PMT) detector. **c** Schematic diagram used for simulating a GNR antenna and a dipole emitter with a polarization state parallel to the length of the antenna

performed time-correlated single-photon counting (TCSPC) measurements using Horiba Scientific Fluoro cube-01-NL. Pulsed picosecond laser diode with pulse duration 70 ps and repetition rate of 1 MHz was used as excitation source. A peak preset of 20,000 counts was used during data collection.

A schematic diagram of the TCSPC setup is shown in Fig. 1b. A polarized laser of 630 nm was incident with a grazing angle, $\sim$ 5° with film sample (Fig. 1b). The grazing angle ensures the large-area excitation of the hybrid; therefore, it increases the total PL intensity and reduces the data collection time. To compare the exciton dynamics of the QD monolayer with isolated and random QDs, we also collected time-resolved photoluminescence spectra of 1:10,000 ratio of GNR and QD hybrid in chloroform after mixing 1 mg/ml of CdSe QDs to 0.1 mg octadecane thiol-capped GNR. Figure 2 shows the time-resolved PL counts collected from the dilute hybrid solution of QDs and GNR optical antenna in chlorofom in a closed cuvette.The data were collected using **p** polarized, along z axis as shown in the Fig. 1b, and **s** (along y axis as shown in Fig. 1b). Here, sample lies in XZ plane. The **p** excitation at 630 nm excites LSPR of AR2 antenna. To extract the life time of excitons in the hybrid of QDs and GNR antenna for both in film and solution, we fitted the decay curve using mostly double- or three-exponential equation if the fitting is not good using the equation $I = I_0 + a_1 e^{\frac{-(t-t_0)}{\tau_1}} + a_2 e^{\frac{-(t-t_0)}{\tau_2}} + a_3 e^{\frac{-(t-t_0)}{\tau_3}}$ where

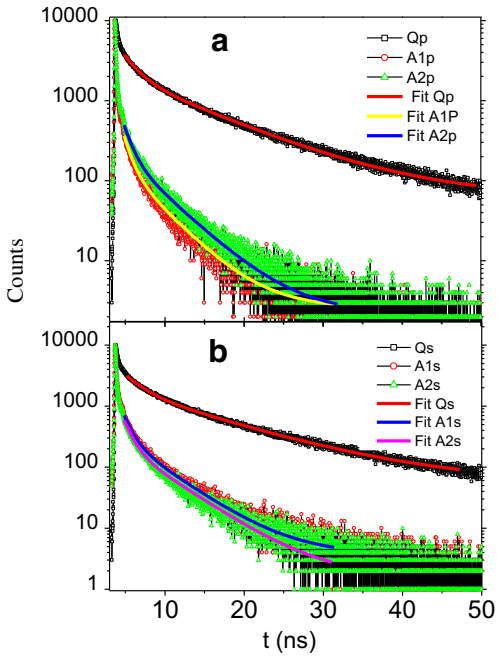

Fig. 2 Log-linear plot of TCSPC data for *solution sample* under (**a**) **p** excitation for QDs in chloroform (Qp), hybrid A1 (A1p); hybrid A2 (A2p) and (**b**) **s** excitation for QDs (Qs), hybrid A1 (A1s); hybrid A2 (A2s). The exponential fit is shown by the thick lines

t_0 and I_0 are offset (shift) values in time (t) and intensity (I) in the data; a_1, a_2, and a_3 are pre-exponential factors; and $\tau 1$, $\tau 2$, and $\tau 3$ are the three components of exciton life time. Mean life time of excitons (τ), for example, for double-exponential decay was calculated as $\left(\tau = \frac{a1\tau^2 + a1\tau^2}{a1\tau + a2\tau}\right)$ [15]. The total decay rate, Γ, for a QD in excited state from the hybrid monolayer can be written in terms of radiative decay rate , Γ_R, and non radiative decay rate Γ_{NR} as $\Gamma = \Gamma_R + \Gamma_{NR}$ and $\Gamma = \frac{1}{\tau}$. Knowing the quantum yield (QY) (10%) of the QDs, we calculated the radiative decay rate using the relation : $QY = \frac{\Gamma_R}{\Gamma}$. Here, we measured the QY in toluene and assumed that it is same for QDs transferred onto the substrates. This is justified assumptions as QY is calculated per unit of QD.

Results and Discussion

From Fig. 2, we can see that the PL decay faster for the hybrid of resonant GNRs (AR2) than the bare QD solutions under both **s** and **p** types of excitation. This is similar to what we observed on film data as shown in Table 2. Although the difference between the mean lifetimes of the QDs in solution under **p** and **s** excitations, in each hybrid (A1 or A2), is not significantly large, it is non zero. This might be due to random motion of GNRs and QDs in the solution. We have also calculated anisotropy in life time defined as, $G_\tau = \left|\frac{\tau_p - \tau_s}{\tau_p + \tau_s}\right|$ where τ_p and τ_s are the average PL life time of CdSe QDs in the hybrid assemblies under **p** and **s** excitations using 630-nm laser respectively. Further, from Table 2, we can see that the anisotropy induced in the A1 hybrid for the solution is threefold larger than the bare CdSe QD solution. This suggests that anisotropy in life time is introduced due to interaction of plasmonic field with QDs (Fig. 2).

To obtain further insight into the mechanism of light matter interaction in hybrid film, we have performed TCSPC measurement on these samples as displayed in Fig. 3. As

Table 2 Average life time τ_{film} and τ_{sol}; radiative decay rate Γ_{R-film} and Γ_{R-sol}; anisotropy in life time $G_{\tau-film}$ and $G_{\tau-sol}$; for QDs (Q) and hybrid A1 and hybrid A2 film and solution respectively for each polarization, P (**p** and **s**)

Sample	P	τ_{fim} (ns)	τ_{sol} (ns)	Γ_{R-film} (ns^{-1})	Γ_{R-sol} (ns^{-1})	$G_{\tau-film}$	$G_{\tau-sol}$
Q	*p*	7.58	9.08	0.0132	0.0110	0.04	0.02
A1	–	4.65	3.39	0.0215	0.0295	0.07	0.06
A2	–	4.45	3.80	0.0225	0.0263	0.04	0.02
Q	s	8.15	9.50	0.0123	0.0105		
A1	–	4.05	3.83	0.0247	0.0261		
A2	–	4.85	3.91	0.2062	0.0256		

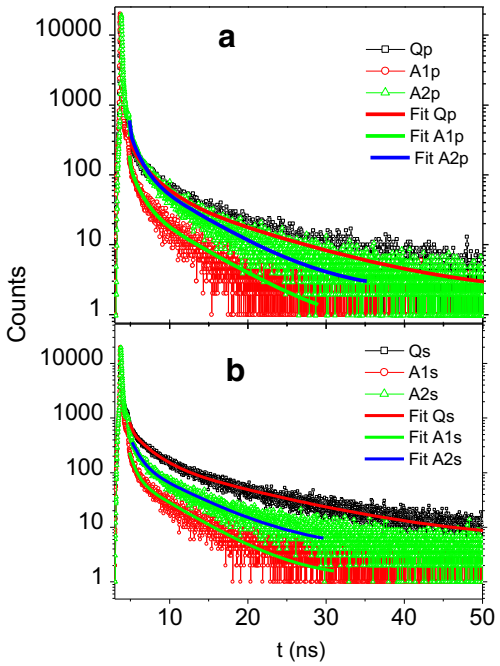

Fig. 3 Log-linear plot of TCSPC data for *film samples* under (**a**) **p** excitation for QDs in chloroform (Qp), hybrid A1 (A1p); hybrid A2 (A2p) and (**b**) **s** excitation for QDs (Qs), hybrid A1 (A1s); hybrid A2 (A2s). The exponential fit is shown by the thick lines

shown in Table 2, reduction of the decay life times in the samples, A1 and A2, is obvious. Further, we observed a twofold enhancement of the radiative decay rate. Again, we observed clear spectral effect in the lifetime anisotropy for A1 samples (resonant excitation). Despite the fact that lifetime measurements have been done with a broad beam and hence the overall orientation alignment of GNR within the illuminated area being much smaller, it is clear that the sample (A1) shows higher lifetime anisotropy than the intrinsic anisotropy of the QD monolayer as shown in Table 2. However, we believe the anisotropy with 633-nm excitation would be stronger if a much smaller-illuminated-area and high-density aligned nanorod antennas are used.

Finite difference time domain (FDTD) simulations (Lumerical solutions) were used to estimate the decay rates for dipoles radiating in the presence of a GNR. The decay rates of the dipole in the presence of resonant (AR1) and off-resonant GNR (AR2) were calculated by measuring the power emitted from the dipole at 660-nm wavelength. The GNR is approximated by a gold cylinder (Fig. 1c), and the optical data for gold is taken from Johnson and Christy [16]. For simulating the lifetime in solution, an averaging over different spatial orientations were done—namely axial, parallel, and normal orientations of a dipole with respect to the nanorod. In case of film, for **p**-polarized excitation, an average of axial and parallel orientations and, for **s**-polarized excitation, the normal orientation were simulated. The size of the simulation region was $1 \times 1\ \mu m^2$, with a uniform mesh of 2 nm over the GNR and a dipole. A broadband plane wave source of intensity 1 $(\frac{W}{m^2})$ is used in all the electric field simulations. Electric field monitors are used to record local fields around the rod. The dipole moment of the source is fixed at 2.8×10^{-31} C-m for all simulations and the wavelength is taken as the emission wavelength of the QD. The electric field modification at the excitation frequency of the QD in the vicinity of a resonant GNR is shown in Fig. 4e–f. We see a strong E field enhancement (22) near GNR antenna and which decay to zero within few nanometer away. For a dipole transition, the decay rate in an inhomogeneous environment is related to the classical power output of the dipole in the same environment by the relation $\frac{\Gamma}{\Gamma_0} = \frac{P}{P_0}$ [5] where Γ is a radiative decay rate, P, P_0 are emission powers of dipole emitters in the presence of the antenna and in the free space respectively. We obtain the normalized total power of the dipole in the presence of the GNR $(\frac{P}{P_0})$, which gives us the normalized total decay rate. The total power emitted by the dipoles is also calculated using power monitors arranged as a box around the dipole. This can be written as the sum of radiated and non radiated power, $P = P_r + P_{nr}$. The rate of transfer (non radiative power) is calculated as the difference of the total power and the radiated power. Normalizing these quantities with the free space values gives the ratios of radiative and non radiative decay rates. $\frac{\Gamma_r}{\Gamma_0} = \frac{P_r}{P_0}$ and $\frac{\Gamma_{nr}}{\Gamma_0} = \frac{P_{nr}}{P_0}$.

From Fig. 4a–d, it is seen that very close to the metal particle, the non radiative decay dominates the radiative process. The radiative rate enhancement for a dipole emitter near a metal nanoparticle is mainly due to coupling with the dipole mode of the surface plasmon, whereas the emitter can couple with all modes of the surface plasmon to transfer energy. At very close distances, the coupling with the higher modes becomes stronger, leading to very high non radiative decay. At larger distances, the coupling with higher modes becomes weak and the radiative processes dominate in this regime. FDTD results show that the modification in decay rates is greater for the resonant system (Fig. 4a, c) as compared to the off-resonant (Fig. 4b, d) system. In solution, the orientations are not fixed and are expected to be random. To know the mean separation between QDs and GNR, we first calculated the mean distance between the QDs, r_{mean}, using the probability distribution of randomly moving QDs and GNRs in chloroform as $r_{mean} = 0.55396n^{-1/3}$ [17] where n is number of QDs per unit volume. Using the known concentration (1 mg/ml) of QDs and the mean radius as 5 nm , r_{mean} turns out to be 80.6 nm. Considering length of GNR as 50 (60) nm in case of AR2 (AR3), the minimum surface to surface separation is 10.3 (5.3) nm. So we have calculated the decay rate enhancement as a function of separation (r) between the dipole emitter and GNR antenna (Fig. 4a–d).

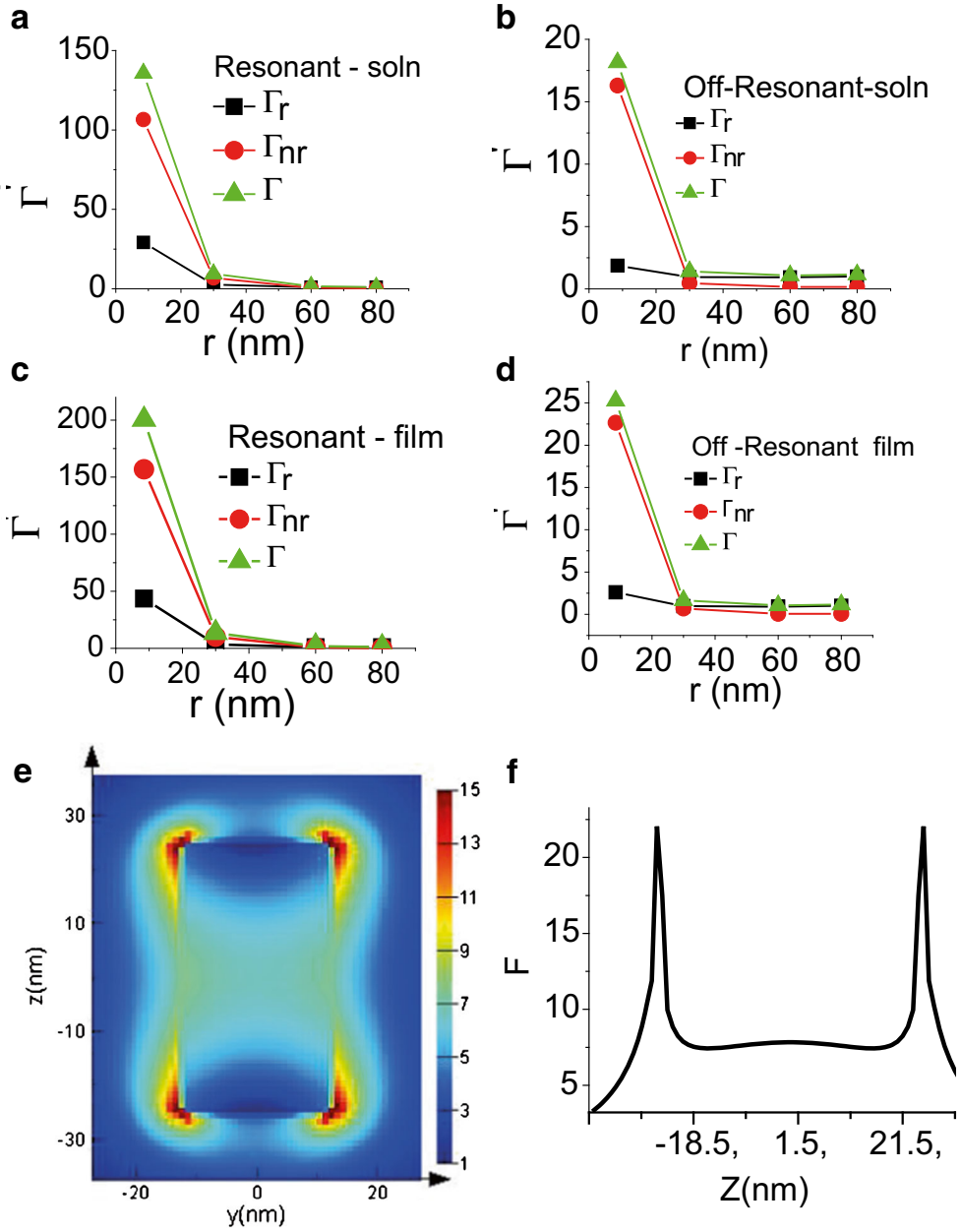

Fig. 4 Calculated decay rate enhancements (Γ') for a dipole in solution and film under **p** excitation as a function of separation between the dipole and **a** GNU antenna AR2 in chloroform, **b** GNR antenna AR3 in chloroform, **c** GNR antenna AR2 in film, and **d** GNR antenna AR3 in film. **e** Electric field enhancement map around a GNR AR2 under **p** excitation. **f** Line profile of electric field enhancement (F) values extracted from **e** along the length of the antenna

The orientation-averaged radiative decay rate enhancement in the hybrid A1 at the separation of 30-nm is found to be 2.6 which is closer to experimental radiative decay rate of 2.7 (Table 2). In comparison, the off-resonant hybrid at 30-nm separation in solution does not show any decay rate enhancement ($\Gamma' \approx 1$). For the close packed film, the resonant system has a mean radiative decay rate enhancement of 3.5 (Fig. 4c) at 30-nm separation for **p** polarization as opposed to experimental radiative decay rate (≈ 2), whereas the decay rates for **s** polarization (not shown here) is almost unchanged. The off-resonant cases show very little deviation from the bare QD system. For the resonant system, the decay rates are more enhanced in the case of **p**-polarized emission as compared to the **s**-polarized case, indicating the role of the longitudinal surface plasmon resonance in modifying the local density of states of the emitter, thereby increasing its emission properties.

In conclusion, in this letter, we provide optimum physical parameters to transfer aligned and low-density GNR antenna over monolayer of QDs and report resonant and off-resonant

GNR antenna-induced radiative and anisotropic decay from the compact monolayer and isolated QDs in solution. We observed enhanced decay rates when the quantum emitters are in the vicinity of the resonant optical antenna. Further, an anisotropic decay was introduced both in the isolated QDs and in the monolayer film by virtue of interaction of the optical antenna. Our fundamental study could be very useful for the scientific community in QD display, quantum communications device, etc.

Acknowledgment We acknowledge the Department of Science and Technology (Nanomission), India, for the financial support and Advanced Facility for Microscopy and Microanalysis, Indian Institute of Science, Bangalore, for access to TEM measurements. M. Praveena acknowledges UGC, India, for the financial support.

References

1. Hoang TB, Akselrod GM, Mikkelsen MH (2016) Ultrafast room-temperature single photon emission from quantum dots coupled to plasmonic nanocavities. Nano Lett 16:270
2. Giannini V, Fernandez-Dominguez AI, Heck SC, Maier SA (2011) Plasmonic nanoantennas: fundamentals and their use in controlling the radiative properties of nanoemitters. Chem Rev 111:3888
3. Novotny L, van Hulst N (2011) Antennas for light. Nat Photonics 5:83
4. Eggleston MS, Messer K, Zhang L, Yablonovitch E, Wu MC (2015) Optical antenna enhanced spontaneous emission. Proc Natl Acad Sci USA 112:1704
5. Novotny L, Hecht B (2006) Principles of nano-optics. Cambridge University Press, Cambridge
6. Bharadwaj P, Deutsch B, Novotny L (2009) Optical antennas. Advances in Optics and Photonics 1:438
7. Neogi A, Morkoç H, Kuroda T, Tackeuchi A (2005) Coupling of spontaneous emission from GaN–AlN quantum dots into silver surface plasmons. Opt Lett 30:93
8. Haridas M, Basu JK, Gosztola DJ, Wiederrecht GP (2010) Photoluminescence spectroscopy and lifetime measurements from self-assembled semiconductor-metal nanoparticle hybrid arrays. Appl Phys Lett 97:83307
9. Russell KJ, Liu T-L, Cui S, Hu EL (2012) Large spontaneous emission enhancement in plasmonic nanocavities. Nat Photonics 6:459
10. Tripathi LN, Praveena M, Basu JK (2013) Plasmonic tuning of photoluminescence from semiconducting quantum dot assemblies. Plasmonics 8:657
11. Haridas M, Tripathi LN, Basu JK (2011) Photoluminescence enhancement and quenching in metal-semiconductor quantum dot hybrid arrays. Appl Phys Lett 98:063305
12. Tripathi LN, Praveena M, Valson P, Basu JK (2014) Long range emission enhancement and anisotropy in coupled quantum dots induced by aligned gold nanoantenna. Appl Phys Lett 105:163106
13. Peng ZA, Peng XG (2001) Formation of high-quality CdTe, CdSe, and CdS nanocrystals using CdO as precursor. J Am Chem Soc 123:183
14. Sau TK, Murphy CJ (2004) Seeded high yield synthesis of short Au nanorods in aqueous solution. Langmuir 20:6414
15. Lakowicz JR (2006) Principles of fluorescence spectroscopy. Springer, Berlin
16. Johnson PB, Christy RW (1972) Optical constants of noble metals. Phys Rev B 6:4370
17. Chandrasekhar S (1943) Stochastic problems in physics and astronomy. Rev Mod Phys 15:1